J. Fluid Mech. (1977), *vol.* 79, *part* 2, *pp.* 391–414
Printed in Great Britain

On cavity flow at high Reynolds numbers

By M. NALLASAMY AND K. KRISHNA PRASAD
Department of Mechanical Engineering, Indian Institute of Science, Bangalore-560012

(Received 6 September 1975 and in revised form 9 August 1976)

The flow in a square cavity is studied by solving the full Navier–Stokes and energy equations numerically, employing finite-difference techniques. Solutions are obtained over a wide range of Reynolds numbers from 0 to 50 000. The solutions show that only at very high Reynolds numbers ($Re \geqslant 30\,000$) does the flow in the cavity completely correspond to that assumed by Batchelor's model for separated flows. The flow and thermal fields at such high Reynolds numbers clearly exhibit a boundary-layer character. For the first time, it is demonstrated that the downstream secondary eddy grows and decays in a manner similar to the upstream one. The upstream and downstream secondary eddies remain completely viscous throughout the range of Reynolds numbers of their existence. It is suggested that the behaviour of the secondary eddies may be characteristic of internal separated flows.

1. Introduction

Several models have been proposed to describe separated flow in the limit of large Reynolds number (see Berger (1971) and Wu (1972) for comprehensive reviews on the subject). This paper concentrates on Batchelor's (1956) constant-vorticity model. The model assumes that the separated region is of fixed extent at high Reynolds numbers; in other words, the size is independent of the Reynolds number. It postulates the existence of a central core of constant vorticity surrounded by a thin viscous layer. The model has not been extensively tested, but is known to be applicable to separated regions with a fixed boundary. A geometry which fulfils this requirement is the cavity.

Cavity flows have attracted considerable attention in recent years because of their many practical implications. Their geometric simplicity lends itself admirably to testing theoretical models and new numerical schemes (which are by far the best means of predicting the characteristics of separated flows). O'Brien (1972) and Bozeman & Dalton (1973) present up-to-date surveys of work on flows in square cavities. We restrict our attention here to some of the important studies to establish the rather unsatisfactory nature of the available results at high Reynolds numbers *vis-à-vis* Batchelor's model.

Burggraf (1966) was the first to study the problem of a square cavity extensively and provide definitive comparisons of Batchelor's model with numerical solutions of the Navier–Stokes equations. The computations, limited to a Reynolds number of 400, show that the flow in a square cavity at low Reynolds

number consists of three eddies: one primary vortex and two secondary eddies. According to Batchelor's model each of these eddies should exhibit a core of uniform vorticity in the limit of infinite Reynolds number. The results of Burggraf show that the primary eddy exhibits a definite trend towards a core of uniform vorticity. But the upstream secondary eddy is found to remain completely viscous even at $Re = 400$. Here one can argue that a Reynolds number of 400 is not high enough to represent adequately the characteristics of the large Reynolds number limit.

The second important study is the experimental work of Pan & Acrivos (1967), which provides some information for Reynolds numbers very much larger than 400. Their results clearly show that the size of the primary vortex is dependent on Reynolds number up to a value of 2700 at least. The upstream corner eddy increases in size up to a Reynolds number of 500 and thereafter shrinks continuously. At a Reynolds number of 2700 (the maximum value investigated) the upstream eddy retreats to the corner, becoming very small, as at $Re = 0$. Thus the secondary eddy does not exhibit a fixed extent at large Reynolds numbers. The growth and decay of the secondary eddy together with the viscous nature observed by Burggraf at $Re = 400$ indicate that the eddy remains viscous throughout the range of Reynolds numbers. These two features of the separated eddy appear to be inconsistent with the concepts of Batchelor's model. In fact, no physically unconstrained closed-streamline flow is known to exhibit a viscous-to-inviscid transition.

It may be pointed out that the experiments of Pan & Acrivos did not exhibit the second eddy at the downstream corner of the cavity which has been noticed in many numerical computations (see, for example, Greenspan 1969; Bozeman & Dalton 1973). While detailed results are not presented by Greenspan, it was clearly demonstrated that the eddy system in a square cavity reduced to a single primary eddy at some Reynolds number between 10^4 and 10^5.

The picture that emerges from the above is that relatively few detailed studies are available on the structure of cavity flows for a wide range of Reynolds numbers. A few broad questions with respect to the characteristics of the secondary eddies, the Reynolds number at which they disappear, the position of the vortex centre as a function of the Reynolds number and finally the limiting value of the vorticity remain unanswered. In other words, no results (numerical or experimental) exist which completely validate the Batchelor model. This paper presents detailed results of numerical solutions to the Navier–Stokes equations governing flows in square cavities which answer all the questions raised above. Heat-transfer results are also presented for one set of boundary conditions on the cavity walls. Lastly, the results are compared with the computations based on Batchelor's model presented by Burggraf.

2. Governing equations

We consider the steady, plane, laminar motion of an incompressible, constant-property, Newtonian fluid in a square cavity. The flow itself is induced by steady motion of one of the walls in its own plane. The moving wall is at a uniform

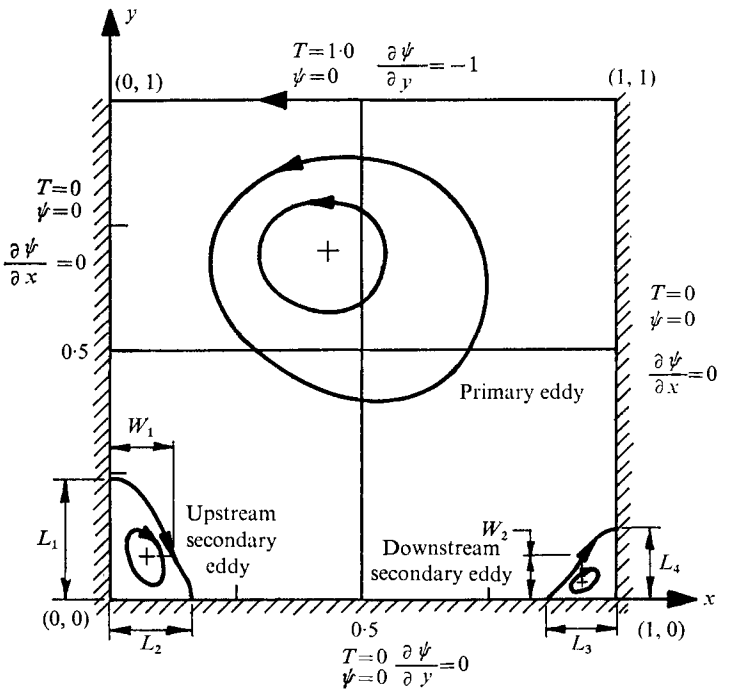

FIGURE 1. Definition sketch.

temperature higher than that of the other three walls, which are also at uniform temperature (see figure 1). This problem is the same as the one studied by many earlier investigators.

The governing equations of the problem are

$$\nabla^2\psi = -\omega, \tag{1}$$

$$\nabla^2\omega = Re\left(\frac{\partial\psi}{\partial y}\frac{\partial\omega}{\partial x} - \frac{\partial\psi}{\partial x}\frac{\partial\omega}{\partial y}\right), \tag{2}$$

$$\nabla^2 T = Re\,Pr\left(\frac{\partial\psi}{\partial y}\frac{\partial T}{\partial x} - \frac{\partial\psi}{\partial x}\frac{\partial T}{\partial y}\right). \tag{3}$$

The boundary conditions to be satisfied are

$$\psi(0,y) = \psi(1,y) = \psi(x,0) = \psi(x,1) = 0, \tag{4}$$

$$\left.\frac{\partial\psi}{\partial x}\right|_{x=0} = \left.\frac{\partial\psi}{\partial x}\right|_{x=1} = \left.\frac{\partial\psi}{\partial y}\right|_{y=0} = 0, \quad \left.\frac{\partial\psi}{\partial y}\right|_{y=1} = -1, \tag{5}$$

$$T(0,y) = T(x,0) = T(1,y) = 0, \quad T(x,1) = 1. \tag{6}$$

In the above equations, ψ, ω and T are the dimensionless stream function, vorticity and temperature and Re and Pr denote the Reynolds and Prandtl numbers respectively.

3. The numerical technique

A detailed description of the numerical technique employed in the present investigation is available elsewhere (Nallasamy & Krishna Prasad 1974). Here we shall mention only a few of its main features. A discrete analogue of (1)–(6) is constructed using the 'upwind' difference scheme, which is known to yield stable solutions up to very high Reynolds numbers. The simultaneous equations generated by the finite-difference scheme are solved by the alternating direction line iterative (ADLI) method developed by the authors. This method combines the advantages of the conventional alternating direction implicit procedure and the line successive over-relaxation procedure. It has been shown to be accurate and reliable for flows up to very high Reynolds numbers, to be economical and is very easy to code.

The convergence criterion used in this investigation is $|(f^{n+1}-f^n)/(f^{n+1})|_{\max} < \epsilon$, where f is the function iterated, n the iteration count and ϵ an arbitrary small number. A value of $\epsilon = 0.5 \times 10^{-2}$ for the vorticity both on the boundary and at interior points gives accurate solutions of the momentum equations. A value of $\epsilon = 0{\cdot}1 \times 10^{-2}$ is chosen for the temperature field. A mesh size of $h = \frac{1}{50}$ is used throughout the investigation and provides adequate spatial resolution.

The computational results on the flow field are used to calculate the total pressure P from

$$\frac{\partial P}{\partial x} = -\omega\frac{\partial \psi}{\partial x} - \frac{1}{Re}\frac{\partial \omega}{\partial y}, \tag{7}$$

$$\frac{\partial P}{\partial y} = -\omega\frac{\partial \psi}{\partial y} + \frac{1}{Re}\frac{\partial \omega}{\partial x}. \tag{8}$$

The reference value for the total pressure is chosen as the value at the centre of the bottom wall. The Prandtl number for the results presented here is unity. All the computations were carried out on an IBM 360/44 System. The results are discussed in the next section.

4. Results and discussion

A large amount of numerical information on the Reynolds number range 0–50 000 has been collected during the present investigation. Some selected results are presented in this section with the particular aim of describing the asymptotic behaviour of cavity flows at high Reynolds numbers.

Secondary vortices

At the outset, we shall consider the process of stabilization of the eddy system in the cavity. The flow in a square cavity at low Reynolds numbers is characterized by three eddies: one occupying the central core and two other, secondary eddies located at the corners of the bottom wall. These corner eddies each exhibit two length scales: L_1 and L_2 for the upstream corner eddy and L_3 and L_4 for the downstream one (see figure 1 for the definitions of these lengths). The variation of

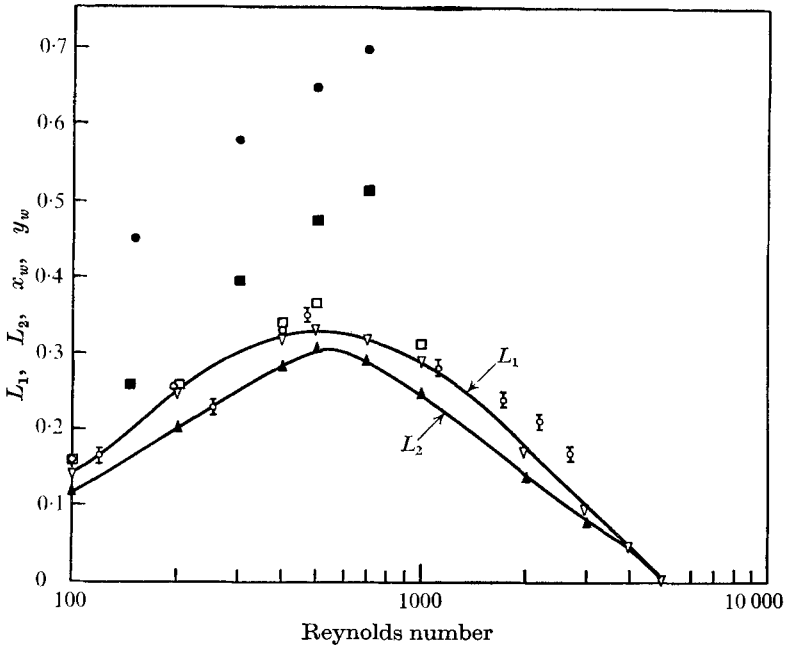

FIGURE 2. Upstream eddy size. ○, Burggraf (1966); □, Bozeman & Dalton (1973); ◊, Pan & Acrivos (1967); ▽, present L_1; ▲, present L_2; ●, x_w, Leal (1973); ■, y_w, Leal (1973).

L_1 and L_2 with Reynolds number is plotted in figure 2. The plot shows that the size of the eddy attains a maximum at a Reynolds number of 500. It is completely obliterated at a Reynolds number of 5000. L_1 and L_2 exhibit a similar behaviour, but L_1 is always larger than L_2. The numerical results of Burggraf (up to $Re = 400$) and Bozemann & Dalton (up to $Re = 1000$) and experimental results of Pan & Acrivos (up to $Re = 2700$) for L_1 are also plotted in this figure. It is seen that the present computations show the best agreement with the experimental findings. All the earlier investigations tacitly assume that one length scale (L_1) is sufficient to characterize the secondary eddy. Such an assumption is not justifiable as can be concluded from the figure. The difference between L_1 and L_2 varies significantly with Reynolds number.

It may be instructive to note here that there have been instances where erroneous solutions showing two major eddies in the cavity were obtained. Runchal & Wolfshtein (1969) obtained two major eddies for a Reynolds number of 10^4, using a mesh size of $\frac{1}{10}$. This erroneous solution was corrected in their later publications (Runchal, Spalding & Wolfshtein 1969; Gosman *et al.* 1969). Bozeman & Dalton (1973) obtained two major eddies at $Re = 10^3$ when they used a unidirectional difference approximation to the convective form (UDC) of the governing differential equation. For the same Re, they obtained only one major eddy on using a unidirectional difference approximation to the divergence form (UDD) of the differential equation. So they conjectured that the solution exhibits one or two major eddies depending on the finite-difference approximation used. But their comparison of the two difference approximations is somewhat confusing

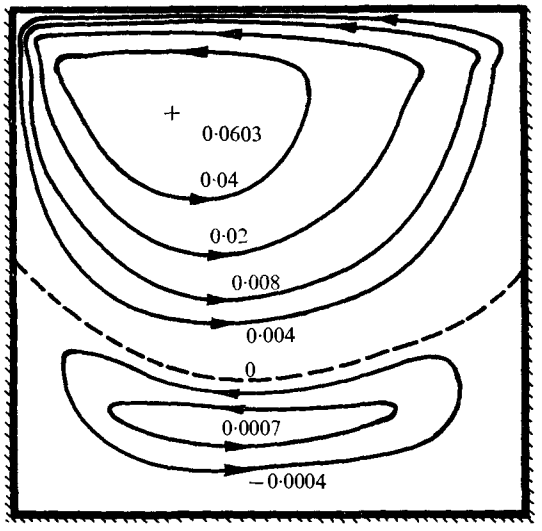

FIGURE 3. Streamline pattern showing two major eddies; $Re = 1000$, $h = \frac{1}{20}$.

for the following reasons: (*a*) they employ different mesh sizes for the two difference approximations, $h = \frac{1}{50}$ for the UDD solution and $h = \frac{1}{80}$ for the UDC solution; (*b*) they state that the reason why Runchal & Wolfshtein obtained two major eddies may be their coarse mesh size.

In an attempt to clear up this confusion, the present authors made a systematic and careful examination of the causes of such erroneous results. This indicated that they are a result of the finite-difference approximations used for the boundary conditions and the manner in which the boundary conditions are satisfied. These factors appear to become insignificant when sufficiently small mesh sizes are used.

As an example, we show an erroneous solution which we obtained by using the same finite-difference approximation (UDC) for the differential equations as in the rest of the present study but a different method of handling the boundary conditions. In the present study, the evaluation of boundary values involved the computation of vorticity values on the boundary and stream-function values at points a distance h from the boundary, as described by Nallasamy & Krishna Prasad (1974), who show that with this method of handling the boundary conditions even a mesh size of $h = \frac{1}{20}$ yields the correct solution (one major eddy) at $Re = 10^3$. In obtaining the solution shown in figure 3, the evaluation of boundary values involved only the computation of the vorticity at the boundary points. The values of the stream function at all the points inside the boundary were computed using a finite-difference form of the differential equation (1). The method of handling the boundary conditions is probably one of the reasons why Bozeman & Dalton's procedure does not yield solutions for Reynolds numbers greater than 1000.

Returning to our discussion of the upstream corner eddy, an important result of the study is that this eddy remains completely viscous throughout the range

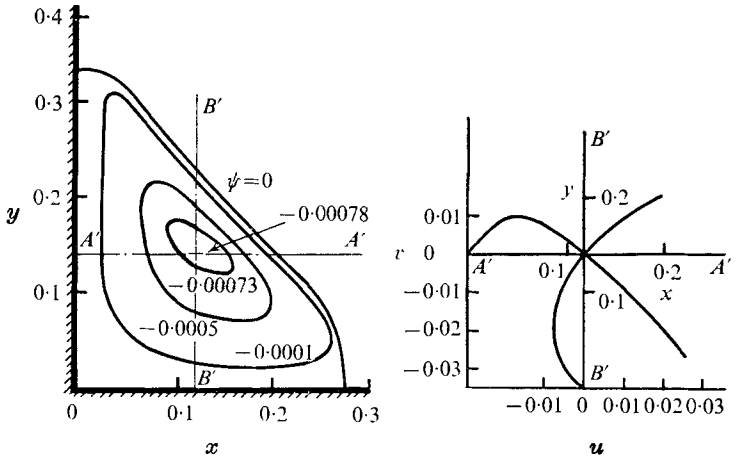

FIGURE 4. Viscous nature of upstream secondary eddy; $Re = 500$.

of Reynolds numbers of its existence. This is best illustrated by plotting the streamline pattern when its size is a maximum. Figure 4 shows such a plot, for $Re = 500$. The streamline pattern shows no sign of the flow becoming inviscid, because in such a case the vortex centre should nearly coincide with the geometric centre of the region and the flow around the centre should be uniform. Further, u and v velocity profiles on the lines through the vortex centre clearly indicate the viscous nature of the flow. As pointed out earlier, Burggraf shows that at $Re = 400$ the upstream eddy is completely viscous in nature. It is worthwhile to recall two related studies on separated flows by Leal (1973) and Grove *et al.* (1964). In his numerical study of separated flow over a finite flat plate Leal observes that the separated flow remains viscous up to a Reynolds number of 800 (the maximum value investigated). In their experiments on flow past a circular cylinder Grove *et al.* find the separated flow to remain viscous even at the maximum value of Re ($\simeq$ 200) attained (i.e. just before flow instability sets in).

The nature of the Navier–Stokes equations demands that a completely viscous region should thin down with increasing Reynolds number. The experimental study of Pan & Acrivos and the present(as well as Bozeman & Dalton's) numerical study show clearly the decrease in size of the upstream eddy at high Reynolds numbers. Further, the present study shows that at sufficiently high Reynolds numbers the physically unconstrained closed-streamline flow (the upstream corner eddy) gradually turns into a thin viscous layer with no recirculation. Here it is worth noting a study by Leal & Acrivos (1969). They consider the flow past a finite plate whose surface moves with a constant velocity U_0 in a direction opposite to that of the free stream (of velocity U_∞). For any velocity ratio U_0/U_∞ the separated region is largest at the smallest Re (based on U_∞ and the length of the plate). With an increase in Re, the size (width) of the separated region decreases.

The size of the downstream corner eddy (characterized by L_3 and L_4) is plotted in figure 5 as a function of Reynolds number. This eddy is small and is practically independent of Reynolds number up to $Re = 500$. Similar behaviour has been

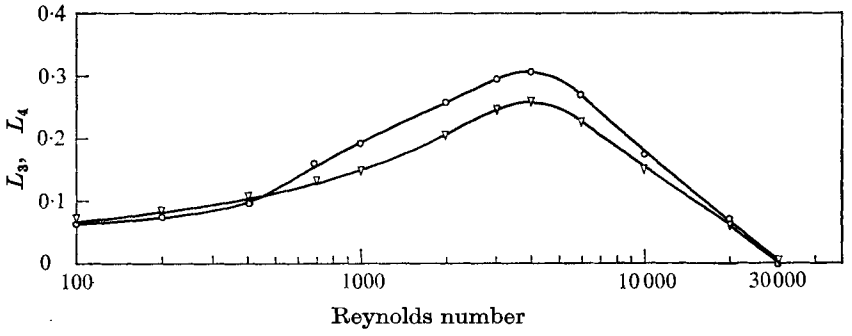

FIGURE 5. Downstream eddy size; present computations. ○, L_3; ▽, L_4.

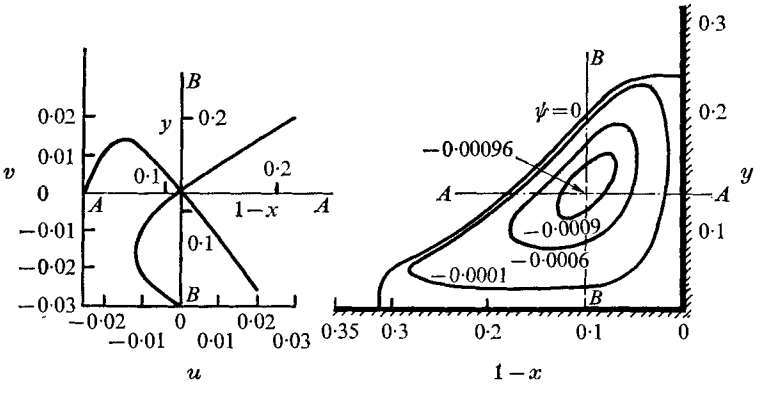

FIGURE 6. Viscous nature of downstream secondary eddy; $Re = 4000$.

reported by Burggraf. As the upstream eddy begins to shrink in size beyond $Re = 500$, the downstream eddy begins to grow; the maximum size of the downstream eddy occurs at $Re = 4000$ (at this value of Re the size of the upstream eddy is insignificant) and it apparently disappears at $Re = 30\,000$. The existence of a downstream corner eddy even after the disappearance of the upstream one is evident in Greenspan's (1969) work (see the figure corresponding to $Re = 10\,000$) as well. Thus it may be seen that the downstream eddy undergoes a growth and decay process similar to that of the upstream one. The downstream eddy's streamwise length L_3 is greater than its cross-stream length L_4 only beyond $Re = 500$. The fact that the downstream corner eddy also remains completely viscous in the range of Reynolds numbers of its existence is illustrated in figure 6. This figure shows the streamline pattern of the eddy at $Re = 4000$ together with the u and v velocity profiles on the lines through the vortex centre.

The relative strengths of the secondary eddies as a function of Reynolds number can be studied by observing the values of the stream function at their centres (table 1). The downstream eddy is very weak up to $Re = 2000$, which is probably the reason why Pan & Acrivos did not observe it in their experiments.

The physical mechanism behind the growth and decay of the secondary eddies can be understood by referring to the streamline patterns in the cavity at $Re = 400$ and 5000, shown in figure 7. At the low Reynolds number end, there is a

	ψ at the centre of the secondary vortices	
Re	Upstream vortex	Downstream vortex
100	$-0{\cdot}241 \times 10^{-4}$	$-0{\cdot}480 \times 10^{-5}$
200	$-0{\cdot}146 \times 10^{-3}$	$-0{\cdot}681 \times 10^{-5}$
400	$-0{\cdot}583 \times 10^{-3}$	$-0{\cdot}169 \times 10^{-4}$
500	$-0{\cdot}782 \times 10^{-3}$	$-0{\cdot}264 \times 10^{-4}$
700	$-0{\cdot}943 \times 10^{-3}$	$-0{\cdot}506 \times 10^{-4}$
1 000	$-0{\cdot}932 \times 10^{-3}$	$-0{\cdot}103 \times 10^{-3}$
2 000	$-0{\cdot}542 \times 10^{-3}$	$-0{\cdot}502 \times 10^{-3}$
3 000	$-0{\cdot}241 \times 10^{-3}$	$-0{\cdot}848 \times 10^{-3}$
4 000	$-0{\cdot}395 \times 10^{-4}$	$-0{\cdot}996 \times 10^{-3}$
5 000	—	$-0{\cdot}990 \times 10^{-3}$
6 000	—	$-0{\cdot}940 \times 10^{-3}$
10 000	—	$-0{\cdot}607 \times 10^{-3}$
20 000	—	$-0{\cdot}194 \times 10^{-3}$
30 000	—	—

TABLE 1. Strength of secondary vortices.

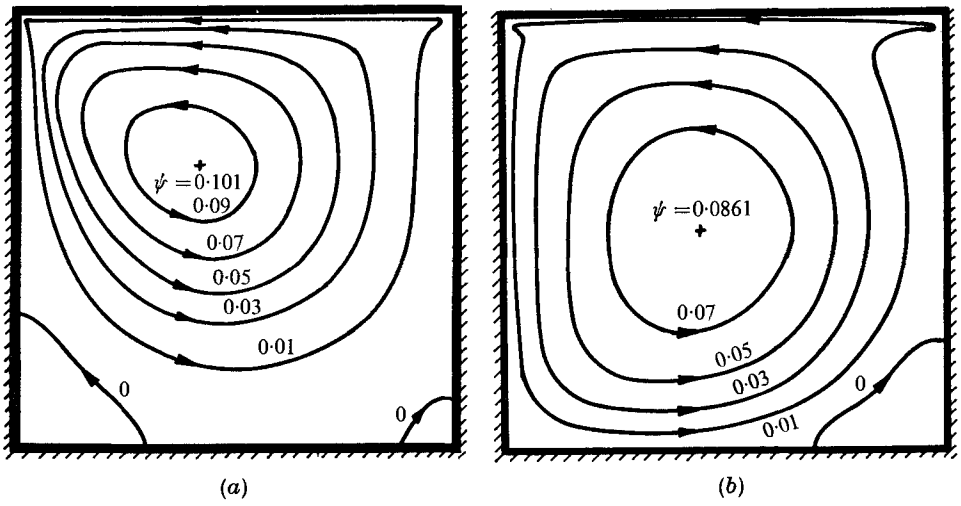

FIGURE 7. Streamline patterns: growth and decay of secondary eddies.
(*a*) $Re = 400$, (*b*) $Re = 5000$.

strong deceleration of the flow along the wall from (0, 1) to (0, 0). At (0, 0), the flow encounters an obstruction which results in a further increase in pressure. The kinetic energy of the fluid stream in the vicinity of the wall at this low Reynolds number is low and the stream is unable to negotiate this pressure hill, with the result that it separates, forming an eddy at the corner. As the Reynolds number increases the stream kinetic energy also increases and hence the eddy shrinks in size, completely disappearing at $Re = 5000$. A similar situation prevails on the bottom wall of the cavity. However, the stream along this wall possesses much smaller kinetic energy by virtue of frictional loss along (0, 1)–(0, 0). Therefore it needs a much larger Reynolds number to overcome the adverse pressure gradient,

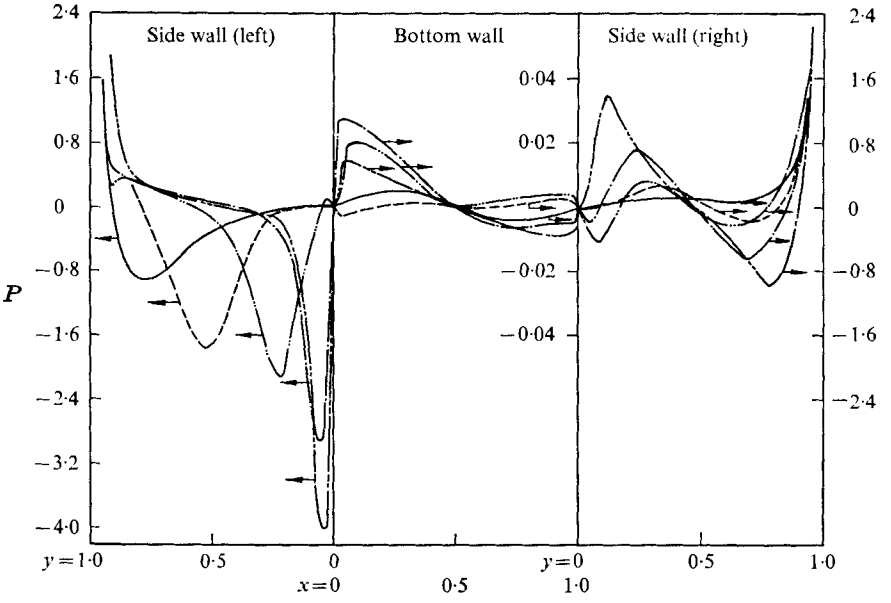

FIGURE 8. Pressure distribution on stationary walls. ——, $Re = 100$; – – –, $Re = 1000$; —··—, $Re = 3000$; —·—, $Re = 10\,000$; ————, $Re = 30\,000$.

hence the observed behaviour of the downstream corner eddy. It may be of interest to note that similar phenomena have been observed by Leal (1973). For a decelerating flow over a flat plate he finds that the length of the separated eddy first increases with Reynolds number but that the rate of increase sharply reduces at larger Reynolds numbers. The variation in its streamwise and cross-stream lengths (x_w and y_w in Leal's paper) with Reynolds number is shown in figure 2. The investigation is limited to $Re = 800$ and it is not known whether the size of the eddy will actually decrease with further increases in Re.

The above nature of the secondary eddies results in a complex variation of the wall pressure. The pressure on the stationary walls is plotted in figure 8 for Reynolds numbers of 100, 1000, 3000, 10 000 and 30 000. It is to be noted that the pressures have been computed with reference to the pressure at the centre of the bottom wall. The pressure on the wall (0, 1)–(0, 0) shows a minimum whose magnitude increases with increasing Re. Also, the point at which the minimum occurs moves towards the corner (0, 0) with increasing Re. At a Reynolds number of 30 000 the point is very near to the corner, indicating that the flow near the wall (0, 1)–(0, 0) no longer encounters strong deceleration due to the corner. The pressure variation on the bottom wall is more complicated because of the existence of upstream and downstream corner eddies. The actual magnitudes of the pressures themselves are small on this wall. (Note the change in scale.) For $Re = 3\,000$ the magnitude of the pressure on the wall is lower than for $Re = 10\,000$. This may be due to the disappearance of the upstream and downstream eddies. The pressure on the wall (0, 1)–(1, 1) shows the accelerating tendency of the flow as it approaches the top moving wall.

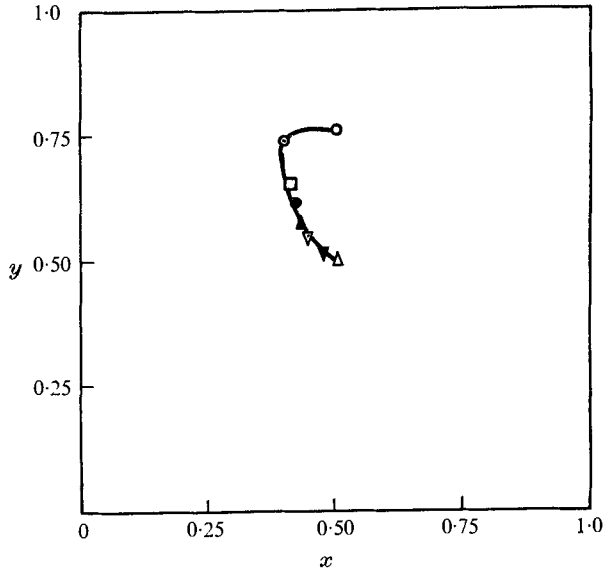

FIGURE 9. Centre of primary vortex. ○, $Re = 0$; ⊙, $Re = 100$; □, $Re = 400$; ●, $Re = 700$; ▲, $Re = 1000$; ▽, $Re = 2000$; ▼, $Re = 10\,000$; ▽, $Re = 30\,000$.

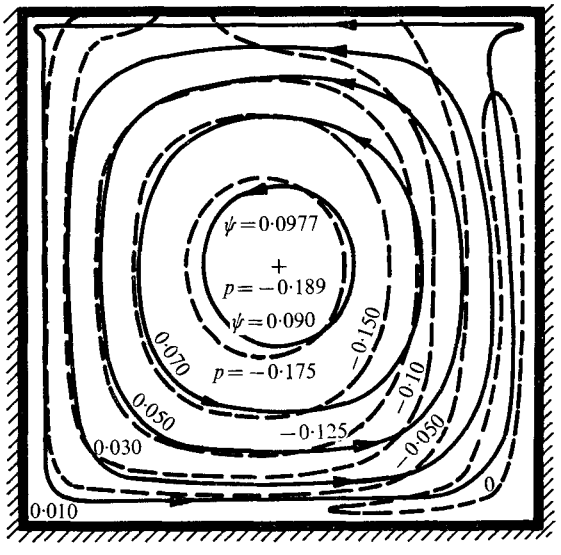

FIGURE 10. Stream function and total-pressure contours; $Re = 30\,000$; – – –, total pressure; ——, streamline.

The behaviour of the primary eddy is studied by noting the location of its centre as a function of Reynolds number (figure 9). At a low Reynolds number of 100, it moves upstream with respect to its location at $Re = 0$; as the Reynolds number is increased, it moves towards the centre of the cavity. The tendency of the vortex centre to move towards the geometric centre has also been reported by Burggraf

as well as Bozeman & Dalton. In addition, Burggraf illustrates that, when a coarse mesh size is employed for the computations, the vortex centre erroneously moves away from the geometric centre with increasing Re. As can be seen from figure 9, no such problem is encountered, even at very high Reynolds numbers, with the mesh size used in the present computations.

Figure 10 shows the streamlines obtained at $Re = 30000$. The flow closely resembles the inviscid flow with the centre of the primary vortex coinciding with the geometric centre of the cavity and the disappearance of the secondary eddies. The first two contours ($\psi = 0{\cdot}09$ and $0{\cdot}07$) enclosing the vortex centre are nearly circular. In the inviscid limit the total pressure is conserved along the streamlines, in which case the total-pressure contours should coincide with the streamlines. The dashed lines represent the total-pressure contours and the close similarity between the two sets of contours in the core region is evident.

Thus if we consider only the primary vortex, it confirms completely Batchelor's constant-vorticity model. Before we examine in greater detail several other features of the cavity flow we digress a little to discuss the reliability of the present computational results.

Reliability of numerical solutions

In finite-difference computations, the major question is whether a chosen mesh size produces an accurate solution. This question is not answerable in general even for simple shapes and linear systems. In practice, the effect of mesh size is ascertained by obtaining solutions with successively smaller mesh sizes. In the present case, a refinement of the mesh, by, say, halving the mesh size, in the entire region is impractical owing to the prohibitive time and memory requirements on the computer (the computer available to the authors simply does not have such storage facilities). No attempt was made to use a graded or non-uniform mesh, since in such a case use of the ADLI method becomes quite complex. The use of successive over-relaxation for high Reynolds number flows results in excessively slow convergence or divergence (Nallasamy & Krishna Prasad 1974). So it was decided to study two specific aspects of the solution, namely, the dependence of the size of the secondary eddies on the mesh size and the effect of mesh size on the main flow.

Regarding the behaviour of the secondary eddies, it was hypothesized that a reduction in mesh size would alter only the Re at which the eddy disappears and not the asymptotic picture. This hypothesis was tested by obtaining solutions with three mesh sizes, $\frac{1}{40}$, $\frac{1}{50}$ and $\frac{1}{60}$, and comparing the eddy sizes. Table 2 shows the sizes of the eddies obtained with the three mesh sizes for $Re = 5000$. A reduction in mesh size from $\frac{1}{50}$ to $\frac{1}{60}$ does not result in the reappearance of the upstream corner eddy and produces only a small change in the size of the downstream eddy. Table 3 shows the sizes of the secondary eddies obtained with the three mesh sizes for high Reynolds numbers. It is seen that, though the actual Re at which the eddy is completely obliterated is progressively increased with improvement in spatial resolution, the picture that as $Re \to \infty$ the separated region tends to disappear is confirmed.

Mesh size h	L_1	L_2	L_3	L_4
$\frac{1}{40}$	—	—	0·261	0·223
$\frac{1}{50}$	—	—	0·288	0·245
$\frac{1}{60}$	—	—	0·296	0·252

TABLE 2. Effect of mesh size: $Re = 5000$.

	$h = \frac{1}{40}$		$h = \frac{1}{50}$		$h = \frac{1}{60}$	
Re	L_3	L_4	L_3	L_4	L_3	L_4
10 000	0·0853	0·0752	0·170	0·147	—	—
20 000	—	—	0·067	0·063	—	—
30 000	—	—	—	—	0·0665	0·0620
40 000	—	—	—	—	0·042	0·039
50 000	—	—	—	—	—	—

TABLE 3. Effect of mesh size: size of the downstream eddy.

Second, the contention that the improvement in spatial resolution will not produce appreciable changes in the main flow was verified for $Re = 30\,000$. Table 4 shows the centre-line u velocities obtained using the three mesh sizes $\frac{1}{40}$, $\frac{1}{50}$ and $\frac{1}{60}$ for $Re = 30\,000$. It is seen that the differences between the two sets of values obtained with $h = \frac{1}{50}$ and $h = \frac{1}{60}$ are considerably smaller than the differences between the results obtained with $h = \frac{1}{40}$ and $\frac{1}{50}$, indicating that $h = \frac{1}{50}$ is sufficiently small. This is also confirmed by the values of the vorticity at the vortex centre at $Re = 30\,000$ obtained with the three mesh sizes. These values are 1·43, 1·27 and 1·30 respectively for the mesh sizes $\frac{1}{40}$, $\frac{1}{50}$ and $\frac{1}{60}$.

Finally, a point of importance in solving the Navier–Stokes equations is that the method should be capable of adequately describing the nature of the boundary-layer flow in regions of the flow where boundary-layer theory applies. To achieve this with a finite-difference technique, the mesh size in these regions must be adjusted in accordance with boundary-layer theory. (Note that this is in contrast to the $Re^{\frac{1}{4}}$ dependence in spectral simulation of laminar flow with a viscous layer; see Orszag & Israel 1974.) In the present problem, the variation of the width of the major viscous regions (the secondary eddies) with $Re^{-\frac{1}{2}}$ (figure 11) shows the following: (*a*) the viscous regions do not exhibit a regular boundary-layer behaviour, i.e. the width does not decrease monotonically as $Re^{-\frac{1}{2}}$ with increasing Reynolds number; (*b*) the range of Re in which the width varies as $Re^{-\frac{1}{2}}$ is different for the upstream and downstream corner eddies. Also, as explained in the previous section, the operating Reynolds number for each eddy appears to be different. If a Reynolds number characteristic of the secondary eddies is defined, a condition like $h\sqrt{Re} < 1$ would be easily satisfied by the mesh size used in the present computation.

Thus the checks show that the asymptotic picture of the separated eddies exhibited by the present study is sufficiently accurate and reliable. In what follows we examine other features of the cavity flow.

y	$h = \frac{1}{40}$	$h = \frac{1}{50}$	$h = \frac{1}{60}$
1·0	−1·0	−1·0	−1·0
0·9	−0·340	−0·317	−0·309
0·8	−0·224	−0·207	−0·207
0·7	−0·136	−0·127	−0·126
0·6	−0·060	−0·060	−0·063
0·5	0	0	0
0·4	+0·075	+0·062	+0·060
0·3	+0·156	+0·135	+0·129
0·2	+0·246	+0·222	+0·216
0·1	+0·364	+0·327	+0·312
0	0	0	0

TABLE 4. Centre-line u velocity: $Re = 30\,000$.

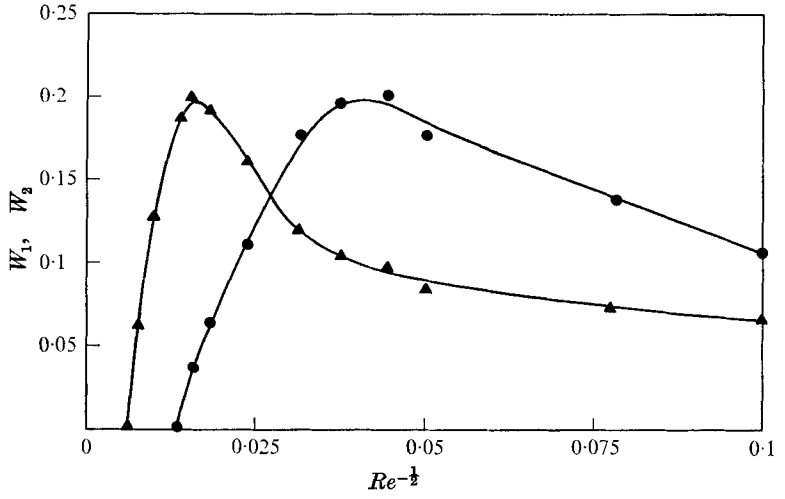

FIGURE 11. Width of the secondary eddy. ●, upstream eddy (W_1); ▲, downstream eddy (W_2).

Velocity and temperature profiles

Figure 12 shows the u velocity profiles on the vertical centre-line ($x = 0{\cdot}5$) and the v velocity profiles on the horizontal centre-line ($y = 0{\cdot}5$) of the cavity for different Reynolds numbers (100, 1000, 10 000 and 30 000). It also includes profiles for fully viscous flow ($Re = 0$) and fully inviscid flow ($Re \to \infty$). The profiles for $Re = 0$ and 100 are well rounded. On the vertical centre-line, the velocity profiles (in the core) in the intermediate range $Re = 200$–1000 are parallel to the inviscid profiles. This result prompted Burggraf to suggest that the slope of the velocity profiles in the core region is independent of Reynolds number. However the profiles at higher Reynolds numbers intersect the inviscid profile at an angle which is a function of the Reynolds number. As a matter of fact the form of the profiles at higher Reynolds numbers indicates that they can be constructed to a good approximation by matching asymptotically the solutions for the boundary layer and the inviscid core. Similar behaviour is observed for

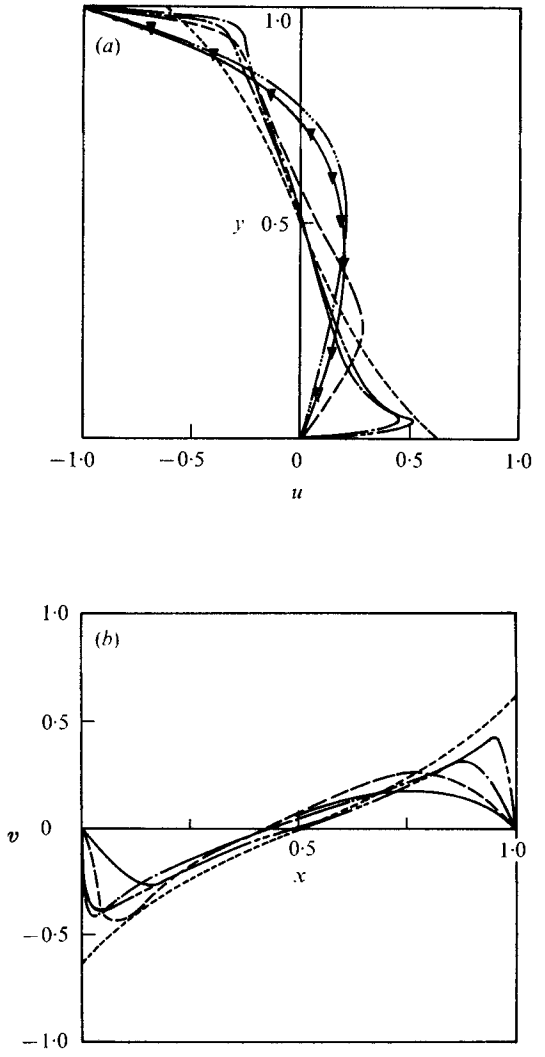

FIGURE 12. Centre-line velocities. (*a*) u velocity on vertical centre-line. (*b*) v velocity on horizontal centre-line. —·—·—, $Re = 0$; ——, $Re = 100$; – – –, $Re = 1000$; - · -, $Re = 10\,000$; — — — —, $Re = 30\,000$; - - -, $Re \to \infty$ (Burggraf 1966).

the v velocity profiles on the horizontal centre-line except that the slope transition discussed above occurs at a much higher Reynolds number. This difference in behaviour is due to the secondary eddy at the downstream corner, which persists up to a very high Reynolds number.

Another interesting feature of the velocity profiles is an overshoot in the region of transition between the viscous layer and the inviscid core. According to Burggraf, this represents a fundamental difference between recirculating flows and single-pass flows. The difference arises because of periodic past history of the boundary layer. Such an explanation seems to us to be somewhat speculative in the light of some of the recent numerical solutions of the Navier–Stokes equations.

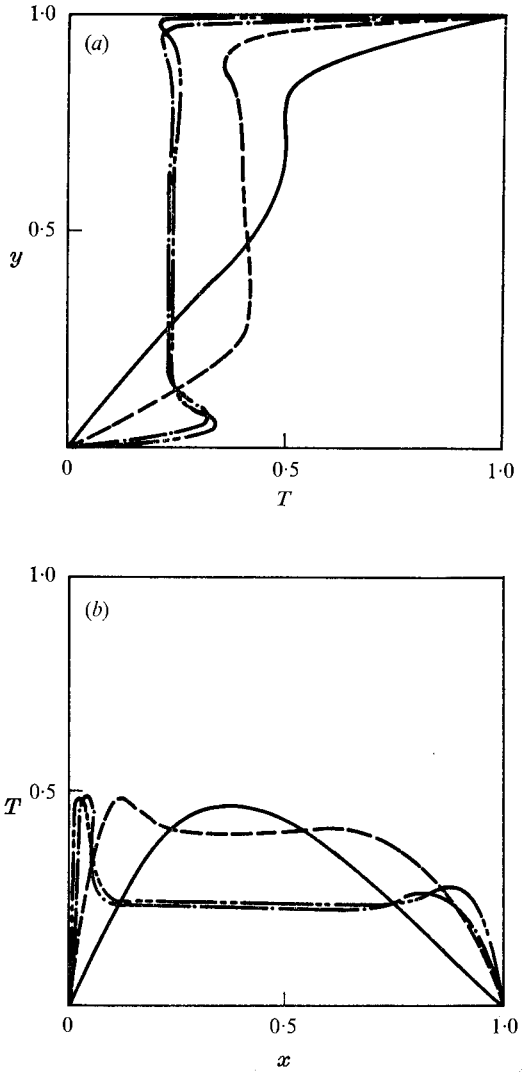

FIGURE 13. Centre-line temperature profiles. (*a*) On vertical centre-line. (*b*) On horizontal centre-line. ——, $Re = 100$; – – –, $Re = 1000$; –·–, $Re = 10\,000$; ———, $Re = 30\,000$.

Similar velocity overshoots are observed in the entrance region of flow in a two-dimensional channel when the solution is constructed numerically from the Navier–Stokes equations (Wang & Longwell 1964; Brandt & Gillis 1966), in full Navier–Stokes solutions of external flows (Mehta & Lavan 1975), and in wind-tunnel experimental velocity profiles (Acrivos *et al.* 1968). It should be noted that this overshoot is smeared if the solution is obtained from the boundary-layer approximation to the problem (see for example Bodia & Osterle 1961; Schlichting 1968, on the entrance flow problem). That this overshoot is not a consequence of the numerical scheme employed but an inherent property of the Navier–Stokes equations has been unambiguously established by Van Dyke (1970) and

Abarbanel *et al.* (1970). The present authors examine the mechanism of this overshoot in a separate publication on the transient flow and heat transfer in the entrance section of a two-dimensional channel (Nallasamy & Krishna Prasad 1976). The main conclusion that emerges from this investigation is that the overshoot is caused by a complex interaction between the diffusion of vorticity in the transverse and streamwise directions respectively. This discussion leads us to conclude that the velocity overshoot is a characteristic exhibited by the Navier–Stokes equations while describing flows with thin boundary layers interacting with inviscid regions.

Application of Bachelor's model to cavity flows will produce smeared velocity profiles as in the boundary-layer solutions for entrance flow. This raises the question of adequacy of the model for practical computations. The experience with entrance flows in two-dimensional channels indicates that the boundary-layer result (though it produces smeared velocity profiles) is an excellent approximation to important engineering quantities such as skin friction. Batchelor's model for cavity flows will likewise serve as an extremely useful and reliable tool for engineering analysis.

Figure 13 shows the temperature profiles on the vertical and horizontal centre-lines of the cavity. The temperature profiles exhibit overshoots similar to those observed in the velocity profiles. It is also clear that the overshoots move towards the wall as the boundary layer thins down (this phenomenon is not very clear with the velocity overshoots because of the complex growth and decay of secondary eddies). The influence of the boundary-layer thickness on the magnitude and position of the overshoot is brought out clearly in studies of transient entrance flow (Nallasamy & Krishna Prasad 1976).

Vorticity and temperature contours

Figure 14 shows the vorticity contours obtained at $Re = 30\,000$. It clearly demonstrates the existence of a constant-vorticity core occupying the major portion of the cavity in conformity with Batchelor's model. The value of the vorticity at the vortex centre is 1·27. This is approximately a third smaller than the limiting value (1·89) computed by Burggraf. In order to establish the reliability of the present result, we list in table 5 the values of the vorticity, the stream function and the pressure coefficient obtained for different Reynolds numbers by Burggraf and in the present investigation. The present results depart from Burggraf's numerical results at $Re = 100$ and 400 by less than 1 %, which can be easily ascribed to the larger mesh size employed by Burggraf. The variation of the vorticity at the vortex centre with Reynolds number is also shown in figure 15. The value of the vorticity goes on decreasing until the corner vortices become insignificant. This is due to the secondary eddies sapping the strength of the primary eddy (Mills 1965). After the disappearance of the corner vortices, the vorticity at the vortex centre increases. For the largest Reynolds number considered in the present investigation (50 000), the vorticity at the vortex centre has a value of 1·45. This is in conformity with the Greenspan value between 1·6 and 1·7 for $Re = 10^5$. These results show the trend towards

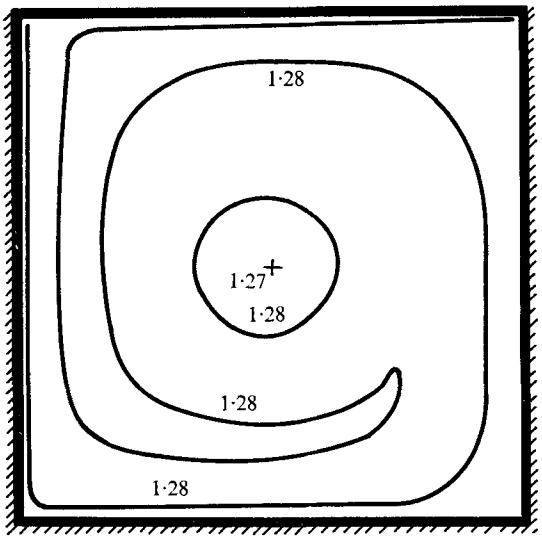

FIGURE 14. Vorticity contours; $Re = 30\,000$.

	Present ($h = \frac{1}{50}$)			Burggraf ($h = \frac{1}{40}$)		
Re	ψ_c	ω_c	$-C_{pc}$	ψ_c	ω_c	$-C_{pc}$
100	0·1026	3·155	0·1844	0·1015	3·143	0·1810
400	0·1014	2·114	0·1820	0·1017	2·142	0·1793
700	0·0986	2·02	0·178			
1 000	0·0977	1·83	0·158			
2 000	0·0951	1·57	0·132			
3 000	0·0906	1·42	0·118			
5 000	0·0861	1·29	0·134			
10 000	0·0873	1·21	0·212			
20 000†	0·0982	1·35	—			
30 000	0·0977	1·27	0·376			
40 000†	0·105	1·39	—			
50 000†	0·108	1·45	—			

† Pressure coefficients have not been computed at these Reynolds numbers.

TABLE 5. Stream function, vorticity and pressure coefficient at the centre of the primary vortex.

a definite limit as $Re \to \infty$. The Burggraf limiting value appears quite plausible in the light of these results. However, Burggraf did not take into account the pressure gradient that is observed in the cavity while calculating the limiting vorticity value. Figure 16 shows the pressure gradient along the walls of the cavity at a Reynolds number of 30 000. Accounting for the pressure gradient should result in a lower value for the vorticity at the vortex centre (see for example Mills 1965).

In the limit $Re \to \infty$, the vorticity and temperature contours should be similar. This implies that the temperature field should be uniform in the core (Burggraf also derives this fact analytically). This is demonstrated in figure 17, which

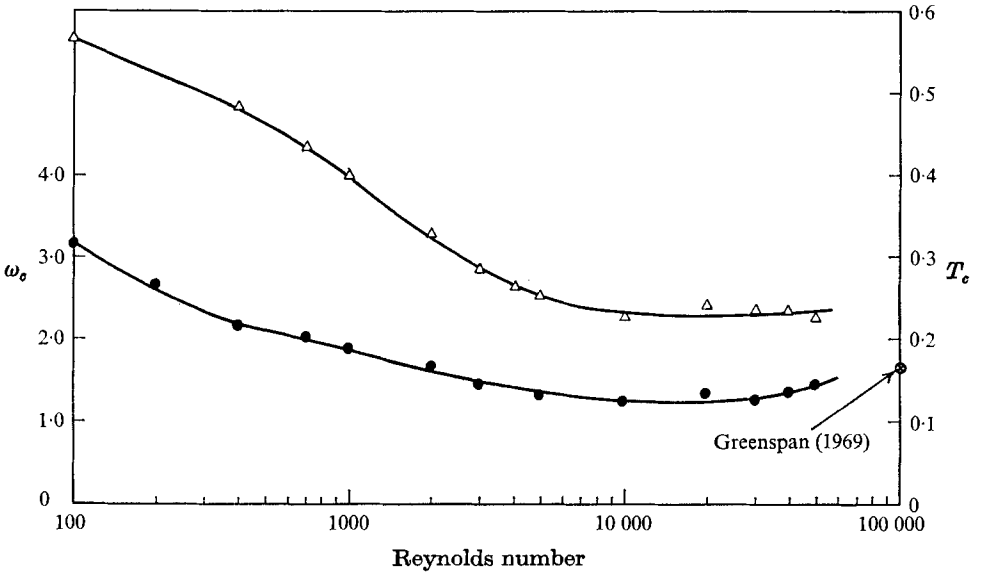

FIGURE 15. Vorticity and temperature at the vortex centre.
△, temperature; ●, vorticity.

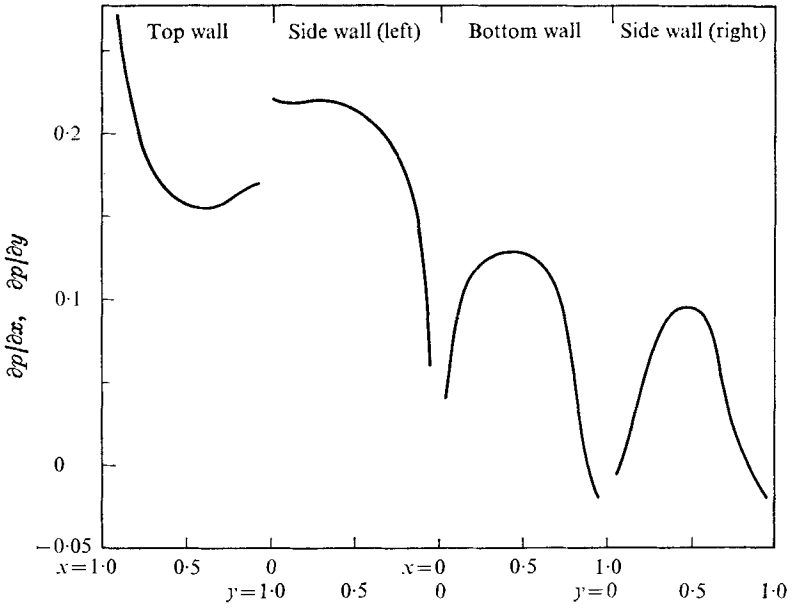

FIGURE 16. Pressure gradient on the walls; Re = 30 000.

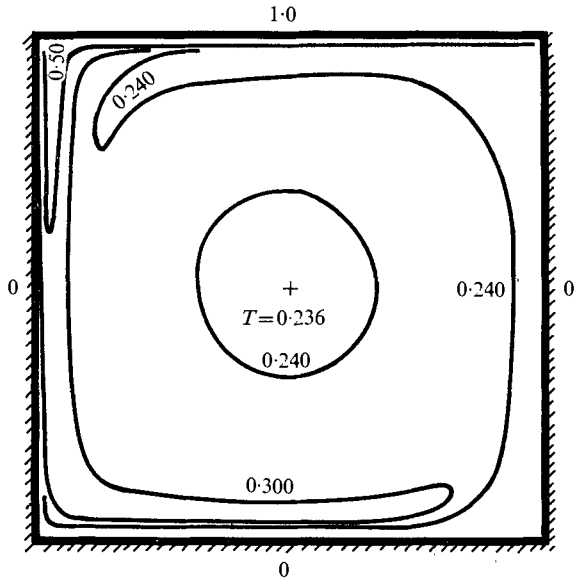

FIGURE 17. Temperature contours; Re = 30 000.

depicts the isotherms, and also by the temperature profiles on the centre-lines of the cavity shown in figure 13. The temperature at the vortex centre, plotted in figure 15, behaves in a manner similar to that of the vorticity at the vortex centre.

Heat-flux results

The variation of the non-dimensional temperature gradient (heat flux) along the walls of the cavity is shown in figures 18 (*a*) and (*b*). Figure 18 (*a*) gives the results for the moving wall at several Reynolds numbers. The result at Re = 100 agrees very well with the numerical results of Burggraf. At larger Reynolds numbers, the heat-flux distributions exhibit a boundary-layer character and furthermore the increase in heat flux at higher Reynolds numbers clearly demonstrates the thinning down of the boundary layer. The heat-flux distributions on all three stationary walls are presented in figure 18 (*b*) to facilitate easy comparison. Again the agreement with the Burggraf numerical computation at Re = 100 is very good. As the Reynolds number is increased, the extent of the region over which the corners influence the heat flux is considerably reduced. The boundary-layer character is clearly brought out by plotting the non-dimensional temperature gradients at the midpoints of the walls against $\sqrt{Re}$ (figure 19). The boundary-layer behaviour at Reynolds numbers of 20 000 and above is evident from the linear variation of the temperature gradient with $\sqrt{Re}$. The slope of the line is different for each wall and goes on decreasing from the upstream moving wall to the downstream side wall. This is due to the decelerating nature of the flow (Evans 1968).

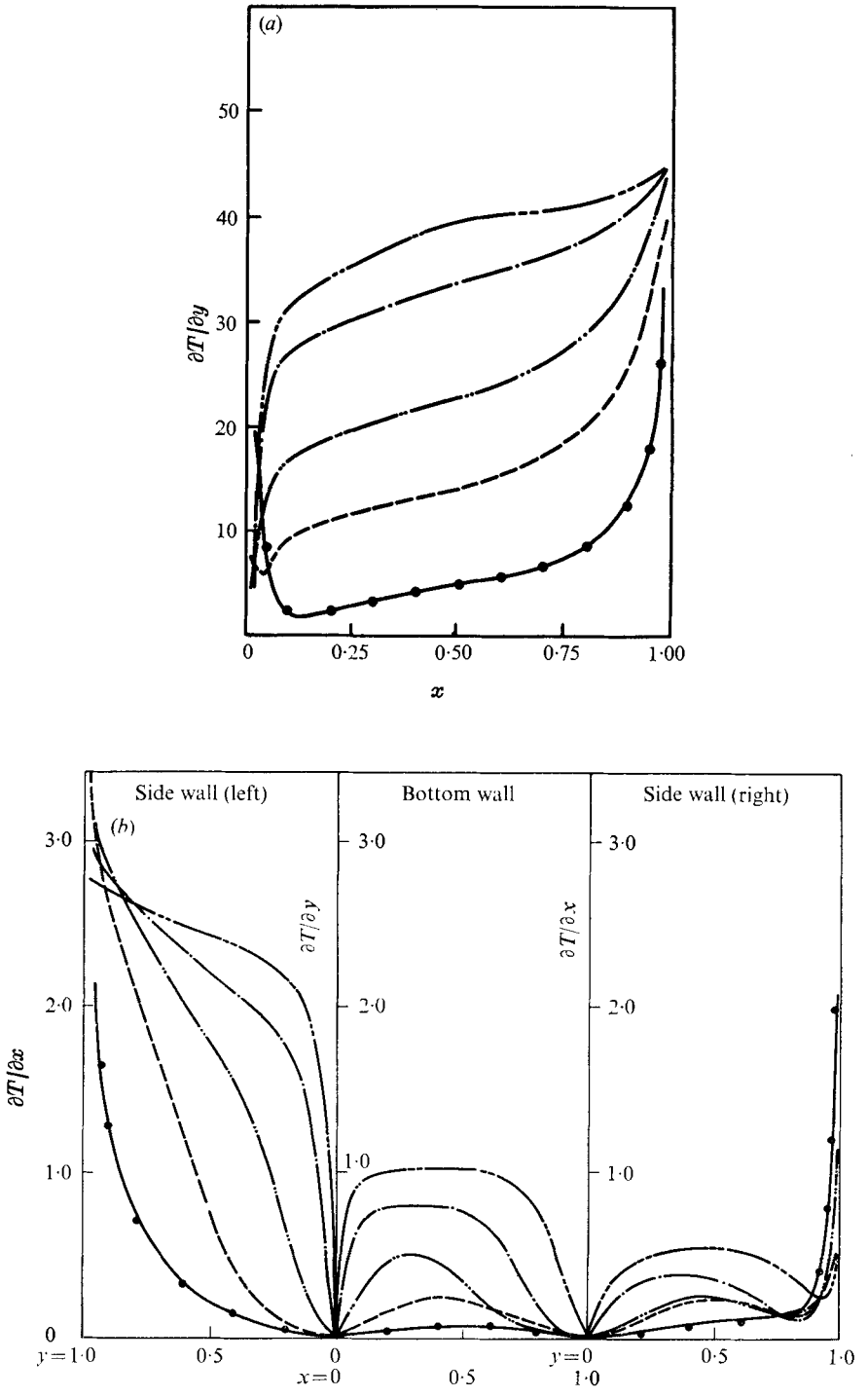

FIGURE 18. Heat flux on (*a*) the moving wall and (*b*) the stationary walls. ——, $Re = 100$; – – –, $Re = 1000$; —··—, $Re = 3000$; —·—, $Re = 10\,000$; – – – –, $Re = 30\,000$; ●, Burggraf (1966).

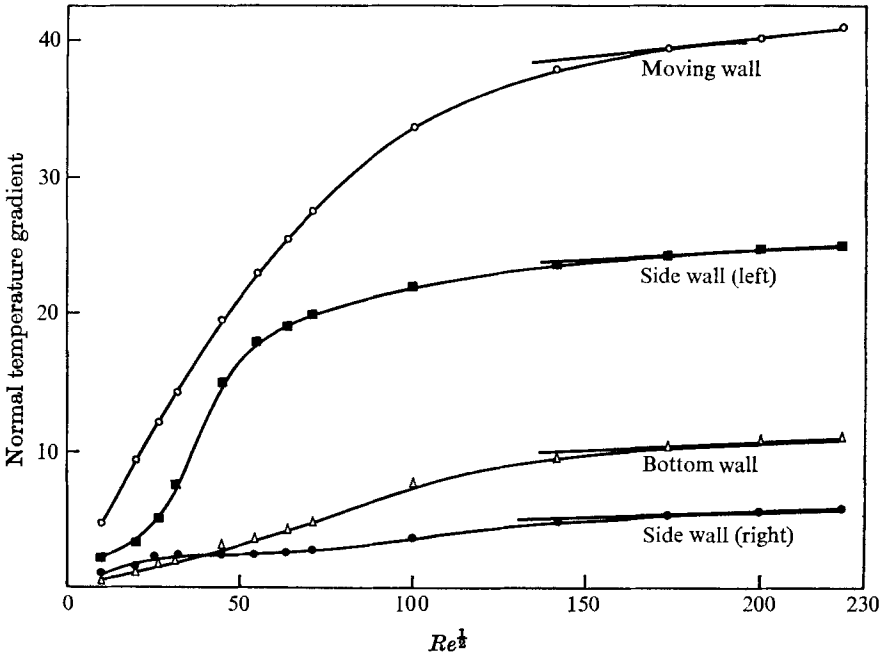

FIGURE 19. Heat flux at the midpoints of the walls.

5. Concluding remarks

A careful examination of the flow in a square cavity at high Reynolds numbers indicates one important feature: the tendency of the secondary eddies to shrink continuously in size. The implications are that the flow in the cavity in the limit of infinite Reynolds number would consist of a single vortex with a constant-vorticity core surrounded by a thin viscous layer as assumed by Batchelor's model. Though we have not been able to establish unambiguously that the secondary eddies disappear at a finite Reynolds number (table 3) owing to the finite mesh sizes employed, the qualitative features of this aspect of the flow are well supported by the agreement of the present results with the experimental results of Pan & Acrivos.

The observed behaviour of secondary eddies opens up two possibilities:

(i) To consider the secondary eddies in the cavity flow as special cases of a very restricted class of separated flows and ignore the present results, saying that they are of little consequence.

(ii) To consider the present picture of the secondary eddies as representative of general laminar separated flows and examine the consequences.

The main reasons compelling one to consider the second possibility are as follows:

(*a*) The reliable picture of the flow that is available in the present study pertains to a range of Reynolds numbers higher than those employed for developing any asymptotic model. (An exhaustive discussion of the existing separated flow models and their limitations is given by Nallasamy 1975.)

(*b*) The qualitative features of the flow obtained in the present study are in agreement with the experimental results of Pan & Acrivos for the same geometry (up to $Re = 2700$), which establishes the growth and decay of separated regions.

(*c*) The secondary eddies remain completely viscous throughout the range of Reynolds numbers of their existence. The viscous nature of separated regions is in conformity with the experimental results of Grove *et al.* (1964) and Acrivos *et al.* (1965, 1968). This seems to suggest that the corner eddies in the cavity flow can be visualized as regions of separated flow produced by an outer flow: the primary vortex.

If we consider the second possibility, the model of separated flow at large Reynolds numbers that emerges is as follows: the laminar separated regions (physically unconstrained closed-streamline flows) remain completely viscous at any Reynolds number; the viscous separated region thins down at large Reynolds numbers and is forced to become a viscous region with no recirculation. This picture of the limiting solution appears to be devoid of any inherent inconsistency.

One way of examining this model in detail would be to study the high Reynolds number solutions for the flow in a rectangular cavity for different aspect ratios. Another is to consider high Reynolds number solutions for other classes of separated regions. Nallasamy (1975) examines the present model in detail for the separated regions in a duct. The results will be discussed in a separate paper.

REFERENCES

Abarbanel, S., Bennet, S., Brandt, A. & Gillis, J. 1970 Velocity profiles of flow at low Reynolds numbers. *J. Appl. Mech., Trans. A.S.M.E.* **37**, 2.

Acrivos, A., Leal, L. G., Snowden, D. D. & Pan, F. 1968 Further experiments on steady separated flow past bluff objects. *J. Fluid Mech.* **34**, 25.

Acrivos, A., Snowden, D. D., Grove, A. S. & Peterson, E. E. 1965 The steady separated flow past a circular cylinder at large Reynolds numbers. *J. Fluid Mech.* **21**, 373.

Batchelor, G. K. 1956 A proposal concerning laminar wakes behind bluff bodies at large Reynolds number. *J. Fluid Mech.* **1**, 388.

Berger, S. A. 1971 *Laminar Wakes.* Elsevier.

Bodia, J. R. & Osterle, J. F. 1961 Finite difference analysis of plane Poiseuille and Couette flow development. *Appl. Sci. Res.* A **13**, 265.

Bozeman, J. D. & Dalton, C. 1973 Numerical study of viscous flow in a cavity. *J. Comp. Phys.* **12**, 348.

Brandt, A. & Gillis, J. 1966 Magnetohydrodynamic flow in the entrance region of a straight channel. *Phys. Fluids*, **9**, 690.

Burggraf, O. R. 1966 Analytical and numerical studies of the structure of steady separated flows. *J. Fluid Mech.* **24**, 113.

Evans, H. L. 1968 *Laminar Boundary-Layer Theory.* Addison-Wesley.

Gosman, A. A., Pun, W. M., Runchal, A. K., Spalding, D. B. & Wolfshtein, M. 1969 *Heat and Mass Transfer in Recirculating Flows.* Academic.

Greenspan, D. 1969 Numerical studies on prototype cavity flow problems. *Comp. J.* **12**, 89.

Grove, A. S., Shair, F. H., Peterson, E. E. & Acrivos, A. 1964 An experimental investigation of the steady separated flow past a circular cylinder. *J. Fluid Mech.* **19**, 60.

Leal, L. G. 1973 Steady separated flow in a linearly decelerated free stream. *J. Fluid Mech.* **59**, 513.

LEAL, L. G. & ACRIVOS, A. 1969 Structure of steady streamline flows within a boundary-layer. High-speed computing in fluid dynamics. *Phys. Fluids Suppl.* **12**, II 105.

MEHTA, U. B. & LAVAN, Z. 1975 Starting vortex, separation bubbles and stall: a numerical study of laminar unsteady flow around an airfoil. *J. Fluid Mech.* **67**, 227.

MILLS, R. D. 1965 Numerical solution of viscous flow equations for a class of closed flows. *J. Roy. Aero. Soc.* **69**, 714.

NALLASAMY, M. 1975 Numerical studies on laminar internal separated flows. Ph.D. thesis, Indian Institute of Science, Bangalore.

NALLASAMY, M. & KRISHNA PRASAD, K. 1974 Numerical studies on quasilinear and linear elliptic equations. *J. Comp. Phys.* **15**, 429.

NALLASAMY, M. & KRISHNA PRASAD, K. 1976 Transient entry flow. To be published.

O'BRIEN, V. 1972 Closed streamlines associated with channel flow over a cavity. *Phys. Fluids*, **15**, 2089.

ORSZAG, S. A. & ISRAEL, M. 1974 Numerical simulation of viscous incompressible flows. *Ann. Rev. Fluid Mech.* **6**, 281.

PAN, F. & ACRIVOS, A. 1967 Steady flow in rectangular cavities. *J. Fluid Mech.* **28**, 643.

RUNCHAL, A. K., SPALDING, D. B. & WOLFSHTEIN, M. 1969 Numerical solution of the elliptic equations for transport of vorticity, heat and matter in two dimensional flow. *Phys. Fluids Suppl.* **12**, II 21.

RUNCHAL, A. K. & WOLFSHTEIN, M. 1969 Numerical integration procedure for steady state Navier–Stokes equations. *J. Mech. Engng Sci.* **11**, 445.

SCHLICHTING, H. 1968 *Boundary Layer Theory*, 6th edn. McGraw-Hill.

VAN DYKE, M. 1970 Entry flow in a channel. *J. Fluid Mech.* **44**, 813.

WANG, Y. L. & LONGWELL, P. A. 1964 Laminar flow in the inlet section of parallel plates. *A.I.Ch. E. J.* **10**, 323.

WU, T. Y. 1972 Cavity and wake flows. *Ann. Rev. Fluid Mech.* **4**, 243.